4172 *Chem. Mater.* **2009,** *21,* 4172–4183
DOI:10.1021/cm900077h

CHEMISTRY OF MATERIALS
Article

Formation of Gold Nanocrystalline Films at the Liquid/Liquid Interface: Comparison of Direct Interfacial Reaction and Interfacial Assembly

Kun Luo,[†,§] Sven L. M. Schroeder,[†,‡] and Robert A. W. Dryfe*[,†]

[†]*School of Chemistry,* [‡]*School of Chemical Engineering & Analytical Science, and University of Manchester, Oxford Road, Manchester M13 9PL, U.K.* [§]*Present address: Department of Materials and Chemical Engineering, Guilin University of Technology, 12 Jiangan Road, Guilin 54004, PR China*

Received January 11, 2009. Revised Manuscript Received July 3, 2009

The formation of gold (Au) nanocrystalline films by reduction at the liquid/liquid interface has been investigated: three product fractions have been characterized, via electron and atomic force microscopy, X-ray photoelectron and UV−vis absorption spectroscopy, and X-ray diffraction. The mechanism suggested is deposition and self-assembly of the Au nanoparticles (NPs) at the liquid/liquid interface occurring in close association with the adsorption of capping ligands obtained from the starting materials and the cleavage of the reducing agent, tetrakis(hydroxymethyl)phosphonium chloride (THPC). NPs can also be assembled at the liquid/liquid interface by adsorption from one of the adjacent solution phases. This parallel route is also followed here to demonstrate that particle formation can occur either via route (i) interfacial reaction or (ii) bulk reaction followed by self-assembly.

Introduction

The liquid/liquid (L/L) interface is a unique environment because of the discontinuity in physical properties the presence of the interface engenders. The interface can be used for the assembly of NPs into solid ultrathin films, owing to its biphasic environment and high mobility of the adsorbates.[1−3] Recent works have discussed the unusual segregation behavior displayed by NP materials when adsorbed at the L/L interface[4] and the use of the interface to prepare unusual nanostructured materials.[5] Preparation of NPs in a controlled form has received significant attention in recent years, with self-assembly offering a convenient approach to achieve the spontaneous self-organization of monolayer-protected NPs into highly ordered structures. Single-electron transfer has been observed in Au NP thin solid films (monolayers or more complicated organized assemblies) prepared by either Langmuir−Blodgett[6] or self-assembly[7] techniques, which offer a significant advance toward the development of nanoparticle-based single-electron transistors (SETs)[8,9] without sophisticated instrumentation. The self-assembly of preformed nanoparticulate materials at L/L interfaces (here defined as L/L self-assembly, LLSA) normally involves the passivation of the NPs by capping molecules, with control over the surface chemistry being used to adjust the contact angle[10−14] of the NPs (with respect to the oil−water interface) to about 90 °. The Gibbs energy (ΔG) of particle adsorption at the L/L interface is given by the following equation:[11]

$$\Delta G = -\pi(d/2)^2\gamma_{L/L}(1 \pm \cos\theta)^2 \qquad (1)$$

where d is the particle diameter, θ is the contact angle, and $\gamma_{L/L}$ represents the tension of the L/L interface. ΔG for nanoscale particles can be comparable to thermal energy (k_BT, k_B is the Boltzmann constant), where the contact angle consequently exerts a strong effect on the adsorption of NPs at L/L interfaces.

*To whom correspondence should be addressed. E-mail: robert.dryfe@manchester.ac.uk.

(1) Glaser, N.; Adams, D. J.; Böker, A.; Krausch, G. *Langmuir* **2006**, *22*, 5227.
(2) Binder, W. H. *Angew. Chem., Int. Ed.* **2005**, *44*, 5172.
(3) Bigioni, T. P.; Lin, X. M.; Nguyen, T. T.; Corwin, E. I.; Witten, T. A.; Jaeger, H. M. *Nat. Mater.* **2006**, *5*, 265.
(4) Lin, Y.; Skaff, H.; Emrick, T.; Dinsmore, A. D.; Russell, T. P. *Science* **2003**, *299*, 226.
(5) Böker, A.; He, J.; Emrick, T.; Russels, T. P. *Soft Matter* **2007**, *3*, 1231.
(6) Pradhan, S.; Sun, J.; Deng, F. J.; Chen, S. W. *Adv. Mater.* **2006**, *18*, 3279.
(7) Feldheim, D. L.; Grabar, K. C.; Natan, M. J.; Mallouk, T. E. *J. Am. Chem. Soc.* **1996**, *118*, 7640.
(8) Bolotin, K. I.; Kuemmeth, F.; Pasupathy, A. N.; Ralph, D. C. *Appl. Phys. Lett.* **2004**, *84*, 3154.
(9) Feldheim, D. L.; Keating, C. D. *Chem. Soc. Rev.* **1998**, *27*, 1.
(10) Binks, B. P.; Clint, J. H.; Fletcher, P. D. I.; Lees, T. J. G.; Taylor, P. *Langmuir* **2006**, *22*, 4100.
(11) Binks, B. P.; Horozov, T. S. *Colloidal Particles at Liquid Interfaces*; Cambridge University Press: Cambridge, UK, 2006; Chapter 1.
(12) Duan, H. W.; Wang, D. A.; Kurth, D. G.; Mohwald, H. *Angew. Chem., Int. Ed.* **2004**, *43*, 5639.
(13) Reincke, F.; Kegel, W. K.; Zhang, H.; Nolte, M.; Wang, D. Y.; Vanmaekelbergh, D.; Mohwald, H. *Phys. Chem. Chem. Phys.* **2006**, *8*, 3828.
(14) Reincke, F.; Hickey, S. G.; Kegel, W. K.; Vanmaekelbergh, D. *Angew. Chem., Int. Ed.* **2004**, *43*, 458.

Published on Web 08/17/2009

L/L interfacial reaction (LLIR) also allows interfacial nucleation and growth of materials, accompanied by ion and/or electron transfer across the interface. It has been reported that gold NPs[15] and platinum NPs[16] can be electrochemically deposited at polarized interfaces between immiscible electrolyte solutions. The role of interfacial tension on nucleation kinetics during electrodeposition at the polarized L/L interface has also been discussed.[17] Previous work from this laboratory has described the deposition[18] of palladium NPs at bare and "templated" L/L interfaces. However, the interfacial deposits tend to agglomerate, and ultrathin NP assemblies have not been obtained by the above approach. In contrast, another approach to LLIR has been described by Rao et al. recently,[19−23] where metal complexes dissolved in toluene spontaneously react with aqueous alkaline solutions containing a reducing agent, tetrakis(hydroxymethyl)-phosphonium chloride (THPC). A wide range of nanocrystalline metallic films (Au, Ag, Pd, and Cu) and alloy films (Au−Ag, Au−Cu, and Au−Ag−Cu) have been reported. Analogous routes allow the preparation of metal chalcogenide films (copper sulphide, cadmium sulphide, and copper selenide) as well as copper oxide, copper hydroxide, and zinc oxide. The presence of capping ligands derived from starting materials affects the morphology of the deposits formed by LLIR. More interestingly, the Au films prepared by LLIR exhibited analogous microstructure to those formed by the LLSA of Au nanoparticles at liquid/liquid interfaces,[12−19] where regular separations among nanocrystalline Au clusters were observed. The similarity suggests a possible connection between these approaches (i.e., LLIR and LLSA). This further highlights the role of capping ligands, which both prevent aggregation and modify the surface of NPs. However, further comparison is not available at present, because both the size of Au NPs and the capping ligands used in the above two approaches were different, and the mechanism of LLIR is not entirely clear. Herein, further investigations into the LLIR process, following Rao's procedure to form Au nanocrystalline films, are described in order to reveal the connection between LLIR and LLSA, the latter involving the assembly of preformed NPs at the L/L interface. To assist mechanistic analysis, hydrazine with selected capping molecules replaced THPC as a reducing agent for the LLIR with $Au(PPh_3)Cl$ in toluene and preformed Au colloid reduced by THPC in alkaline aqueous solution were self-assembled at toluene/water interfaces. The products were characterized with scanning electron microscopy (SEM), atomic force microscopy (AFM), transmission electron microscopy (TEM), X-ray diffraction (XRD), X-ray photoelectron spectroscopy (XPS), and ultraviolet−visible (UV−vis) absorption spectroscopy. Nuclear magnetic resonance (NMR) spectroscopy and cyclic voltammetry were also employed to investigate the decomposition of THPC.

Experimental Section

Chemicals. Chloro(triphenylphosphine)gold(I) ($Au(PPh_3)Cl$, Aldrich), sodium tetrachloroaurate(III) dihydrate ($NaAuCl_4$, 99%, Aldrich), tetrakis(hydroxylmethyl)phosphonium chloride (THPC, 80% aqueous solution, Aldrich), triphenyl phosphine (PPh_3, 99%, Aldrich), tris(hydroxymethyl)phosphine (THP, 95%, Acros Organics), hydrazine (98%, Alfa Aesar), formaldehyde (37% aqueous solution, Aldrich), and lithium chloride (LiCl, 99%, Aldrich) were used as received. Toluene (99%, Fisher Scientific) was employed as the organic solvent in the biphasic experiments, except in some cases of contact angle measurement where 1,2-dichloroethane (DCE, spectrophotometric grade, Sigma) was used. Sodium hydroxide (NaOH, 99.99%, Aldrich) was dissolved in deionized water from an Elga "Purelab Ultra" (Elga, Marlow, U.K.) system to prepare the aqueous alkaline solutions. 0.05 M aqueous solutions of THPC, hydrazine and formaldehyde were prepared separately as reducing agents. The solution containing tris(hydroxymethyl)phosphine oxide (THPO) was prepared by the oxidation of THP in alkaline solution according to the method of Lorenzini et al.,[24] where 8 mL of 1 mM THP solution was adjusted to pH 11.7 by the dropwise addition of concentrated NaOH solution, and kept at room temperature for 72 h.

LLIR Interfacial Deposition Process. Typically, 5 mL of a 1.5 mM $Au(PPh_3)Cl$ solution in toluene and 8 mL of 31.25 mM NaOH solution were added to a glass tube of size 75 mm (height) ×25 mm (diameter). A 165 μL portion of 50 mM THPC solution was injected into the aqueous phase after the L/L interface had stabilized, then the mixture was kept still at ambient temperature.[19,23,25] The reaction was observed over a period of at least 48 h. Three product fractions were observed during this preparation:

Fraction 1 was the interfacial deposit, which was transferred onto glass slides after 24 h of reaction and dried in air. This fraction was subsequently rinsed with acetone and deionized water and dried again at ambient temperature before further analysis.

Fraction 2 was extracted from the toluene solution that had turned brown after 48 h of reaction; the brown product was extracted as discussed below. It was characterized in both liquid and solid (by evaporating toluene) states

Fraction 3 was the coating on the inner wall of the glass tube in contact with the toluene phase. It was rinsed and dried following the same procedure as fraction 1.

Several variations on the default procedure were additionally performed, as follows:

Variation 1a/1b. Alternative reducing agents were employed to probe the effect of the reducing agent (THPC, in the above

(15) Cheng, Y. F.; Schiffrin, D. J. *J. Chem. Soc., Faraday Trans* **1996**, *92*, 3865.
(16) Trojanek, A.; Langmaier, J.; Samec, Z. *J. Electroanal. Chem.* **2007**, *599*, 160.
(17) Johans, C.; Liljeroth, P.; Kontturi, K. S. *Phys. Chem. Chem. Phys.* **2002**, *4*, 1071.
(18) Dryfe, R. A. W.; Simm, A. O.; Kralj, B. *J. Am. Chem. Soc.* **2003**, *125*, 13014.
(19) Rao, C. N. R.; Kulkarni, G. U.; Agrawal, V. V.; Gautam, U. K.; Ghosh, M.; Tumkurkar, U. *J. Colloid Interface Sci.* **2005**, *289*, 305.
(20) Agrawal, V. V.; Mahalakshmi, P.; Kulkarni, G. U.; Rao, C. N. R. *Langmuir* **2006**, *22*, 1846.
(21) Gautam, U. K.; Ghosh, M.; Rao, C. N. R. *Chem. Phys. Lett.* **2003**, *381*, 1.
(22) Gautam, U. K.; Ghosh, M.; Rao, C. N. R. *Langmuir* **2004**, *20*, 10775.
(23) Rao, C. N. R.; Kulkarni, G. U.; Thomas, P. J.; Agrawal, V. V.; Saravanan, P. *J. Phys. Chem. B* **2003**, *107*, 7391.
(24) Lorenzini, F.; Patrick, B. O.; James, B. R. *Dalton Trans.* **2007**, 3224.
(25) Rao, C. N. R. *Curr. Sci.* **2001**, *81*, 1030.

Table 1. Summary of Preparation Procedures Used for LLIR and LLSA Deposition

abbreviation for procedure	locus of reaction	variation
LLIR (fraction 1)	interface, deposit extracted from interface	
LLIR (fraction 2)	interface, deposit extracted from organic phase	
LLIR (fraction 3)	interface, deposit extracted from vessel wall	
LLIR variation 1a	interfacial reaction	CH_2O as reducing agent (replacing THPC)
LLIR variation 1b	interfacial reaction	N_2H_4 as reducing agent (replacing THPC)
LLIR variation 2	interfacial reaction	excess PPh_3 present (THPC reducing agent)
LLIR variation 3a	interfacial reaction	N_2H_4 as reducing agent, in presence of THP
LLIR variation 3b	interfacial reaction	N_2H_4 as reducing agent, in presence of THPO
LLSA variation 1	hydrosol formed, assemble at interface	organic phase: pure toluene
LLSA variation 2	hydrosol formed, assemble at interface	PPh_3 added to organic phase

default procedure). Specifically formaldehyde and hydrazine, (variations 1a and 1b, respectively) were used to reduce Au(PPh_3)Cl via LLIR using the same concentrations and procedure of the above default operation.

Variation 2. An excess amount of PPh_3 (5 mM) was also added to the 1.5 mM Au(PPh_3)Cl toluene solution in some cases, to probe the role of this ligand in stabilizing the nanoparticulate products.

Variation 3a/3b. To determine the source of the capping molecules, and specifically the role of THPC, 1 mM hydrazine in alkaline aqueous solution, with 1 mM THP (at pH 7.32—variation 3a) or THPO (at pH 11.7—variation 3b), were allowed to react with Au(PPh_3)Cl in toluene.

LLSA Process. The LLSA process involves the self-assembly of preformed Au NPs at the toluene/water interface. A 165 μL portion of 0.05 M THPC solution were injected into 8 mL of 6.25 mM NaOH solution, and left to stand for 5 min before adding 3 mL of aged 3.3 mM $NaAuCl_4$ solution into the mixture. The solution turned dark brown after vigorous stirring for 10 min, indicative of the formation of the Au aqueous sol: this monophasic Au reduction with THPC has previously been reported by Duff et al.[26] The sol was then mixed with the same proportion of toluene (denoted as LLSA variation 1) or with 5 mM PPh_3 in toluene solution (LLSA variation 2). After vigorous shaking, the interfacial deposits (with/without PPh_3) were transferred to a glass slide, and rinsed following the procedure used for the LLIR product given above. The various preparation conditions for LLIR and LLSA are summarized in Table 1.

Analytical Techniques. In situ optical microscopy was performed using a Leica DMIL optical microscope fitted with a Sony CCD-IRIS camera on an antivibration system (active vibration isolation system TS-200, HWL Scientific Instruments GmbH). A USB2000 fiber optic UV−vis spectrometer along with CUV sample holder (Ocean Optics Inc.) was employed to record the absorption spectra of the deposits on glass slides (using the same glass slide before deposition as the reference spectrum) and the Au aqueous sol (using the unreacted $NaAuCl_4$ solution as reference). An atomic force microscope (AFM, QScope 250, Quesant Instrument Corporation, $x-y$ translation of 80×80 μm and z translation of 8 μm) was used to analyze the morphology and thickness of the interfacial deposits. X-ray diffraction (XRD) analysis was carried out by an Oxford diffraction system (Xcalibur 2, Mo Kα = 0.7093 Å). XL 30 FEG Philips and ESEM XL30 Philips electron microscopes were employed at 10 kV for scanning electron microscopy (SEM). Transmission electron microscopy (TEM) and high resolution transmission microscopy (HRTEM) were performed with a Tecnai F30 FEG-TEM system operating at 300 kV. The water/toluene/glass three-phase contact angle measurement (see the Supporting Information) was performed on a DSA contact angle measuring system (Kruss GmbH) with DSA 1 drop shape analysis software, by the sessile drop fitting method at ambient temperature.

High-resolution X-ray photoelectron spectroscopy (XPS) was performed with a Kratos Axis Ultra electron spectrometer with a monochromated Al Kα source ($h\nu$ = 1486.6 eV) operating at 180 W and the analyzer operating in CAE mode with a pass energy of 20 eV. Before recording the spectra, the samples were degassed in a load lock chamber at a pressure $< 10^{-6}$ mbar. The vacuum in the spectrometer chamber was $< 10^{-8}$ mbar. The charge neutralization system of the Kratos system was used during data acquisition. The spectrometer energy scale was calibrated according to ISO 15427.[27] Fitting analysis of the data was performed with the XPSPeak 4.1 package, using Gaussian/Lorentzian lines with 20% Gauss character. For the analysis of the P 2p and Au 4f data, spin−orbit splittings of 0.87[28,29] and 3.68 eV[30] were assumed, respectively. The Shirley method[31] was used to model the spectral background. The contribution from adventitious saturated hydrocarbons at 284.8 eV was identified in the C 1s spectra[32] and used as the binding energy reference.

^{31}P NMR spectra were recorded on a Bruker DPX 200 spectrometer operating at 81.01 MHz. THPC solutions were adjusted, with concentrated LiOH solution, to different pH values and left to stand overnight. The measurements were internally referenced to H_3PO_4, and the solvent used for the THPC samples was D_2O. Cyclic voltammetry (CV) was also performed to investigate the time-dependent decomposition of fresh 10 mM formaldehyde and THPC aqueous solutions in the presence of 0.1 M LiCl and 31.25 mM NaOH. The solutions were degassed with pure argon prior to experimentation. A PGSTAT30 potentiostat/galvanostat (Autolab, Eco Chemie B. V.) was used to control the three-electrode cell, where a 2 mm diameter Pt disk was used as the working electrode and Pt mesh and Ag/AgCl wire (homemade) served as counter and reference electrodes, respectively.

Results and Discussions

LLIR Deposit Morphology: Optical and Microscopic Characterization. *Default Preparation*. The approach to

(26) Duff, D. G.; Baiker, A.; Edwards, P. P. *J. Chem. Soc., Chem. Commun*. **1993**, 96.

(27) Seah, M. P. *Surf. Interface Anal*. **2001**, *31*, 721.
(28) Taniguchi, M.; Suga, S.; Seki, M.; Sakamoto, H.; Kanzaki, H.; Akahama, Y.; Terada, S.; Endo, S.; Narita, S. *Solid State Commun*. **1983**, *45*, 59.
(29) Wilke, W. G.; Hinkel, V.; Theis, W.; Horn, K. *Phys. Rev. B* **1989**, *40*, 9824.
(30) Willneff, E. A.; Braun, S.; Rosenthal, D.; Bluhm, H.; Hävecker, M.; Kleimenov, E.; Knop-Gericke, A.; Schlögl, R.; Schroeder, S. L. M. *J. Am. Chem. Soc*. **2006**, *128*, 12052.
(31) Shirley, D. A. *Phys. Rev. B* **1972**, *5*, 4709.
(32) Stevens, J. S.; Schroeder, S. L. M. *Surf. Interface Anal*. **2009**, *41*, 453.

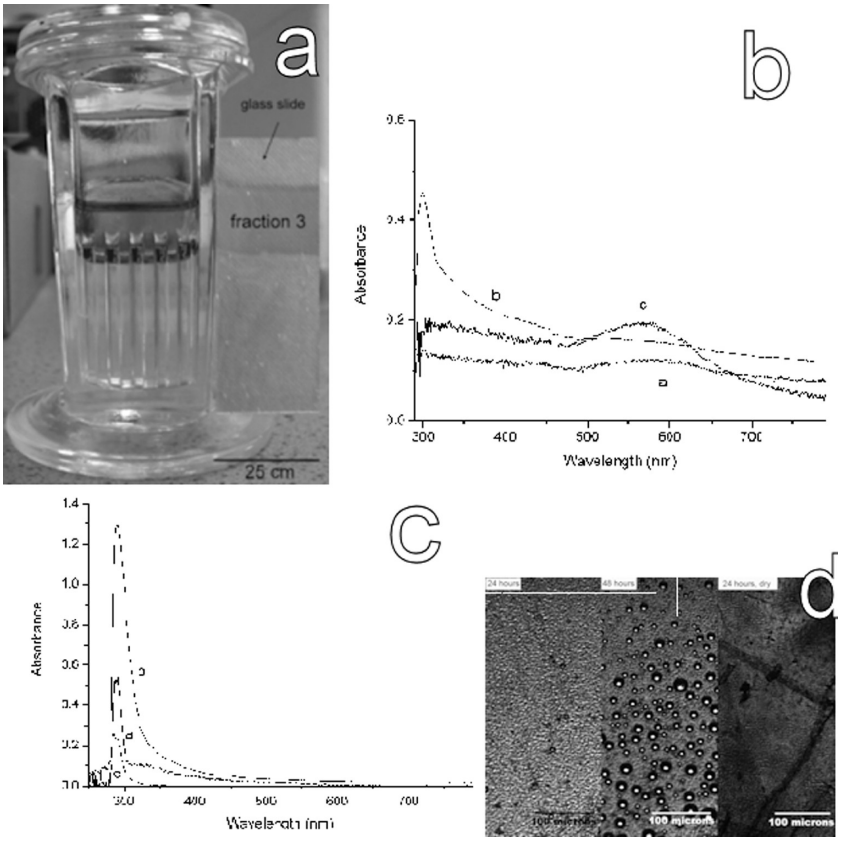

Figure 1. LLIR process and its product. (a) LLIR system after long-term reaction (shown in the glass container) and fraction 3 collected on the glass slide. (b) UV−vis spectra of the solid fractions of the LLIR product: (a) fraction 1, (b) fraction 2, and (c) fraction 3. (c) UV−vis spectra of the organic solution after reaction: (a) fraction 2, (b) $Au(PPh_3)Cl$, and (c) PPh_3. (d) In-situ microscopy of the interfacial deposit at 24 (left) and 48 h (middle) typical LLIR, as well as the dried film at 24 h on the surface of a glass slide (right).

the LLIR previously pursued by Rao et al.[23] was followed here: various products isolated during the LLIR process were analyzed to shed light on the mechanistic details of this process. Small bubbles evolved almost immediately when the THPC solution was injected into the NaOH solution, indicative of the fast cleavage of THPC. After a ca. 10 min induction period, the L/L interface became blurred, and sometimes wrinkles were visible, implying that a thin-film was depositing at the L/L interface. A brown film was visible after approximately 2 h of reaction, and at about 24 h a robust yellow film (fraction 1 from the LLIR process) was seen to form at the L/L interface. The formation of fractions 2 and 3 required a longer period of reaction (approximately 48 h). After removal of the liquid contents (containing fraction 2), as described in the Experimental Section, a coating was observed on the inner wall of the glass tube in contact with the toluene solution (fraction 3). This film was coated on to a removable glass slide placed across the L/L interface before the LLIR started, as shown in Figure 1a.

The above observations indicate that there is an evolution of the LLIR product(s) with time. To determine whether this evolution was reflected by the properties of the three fractions, they were characterized by UV−vis spectroscopy. Figure 1b shows the spectra corresponding to fractions 1 and 3, where pronounced maxima occur at a wavelength of about 570 nm, which is characteristic for the presence on Au nanoparticles. The brown product obtained by evaporation of the toluene solution (fraction 2) is characterized by only a weak absorbance plateau in the region around 570 nm, indicative of the presence of some Au nanocrystal aggregates. However, a stronger absorption band is seen at a wavelength of about 300 nm. This absorption coincides with the main absorption band in the UV−vis spectra of 1.5 mM $Au(PPh_3)Cl$ and 5 mM PPh_3 toluene solutions (Figure 1c). It appears that either $Au(PPh_3)Cl$ or PPh_3 are present in fraction 2. The weak absorption band of the Au nanoparticles extends to ca. 450 nm and imparts the brown color to the toluene solution after long-term LLIR. Therefore, it is reasonable to believe that there are some Au NPs suspended in fraction 2, which aggregate as the toluene solution evaporates.

In situ optical microscopic observation of fraction 1 further reveals that large particles appeared after 48 h of reaction (Figure 1d) which coarsened the interfacial layer compared to 24 h of reaction. Figure 1d also demonstrates that the interfacial deposit (fraction 1), when transferred to the glass slide, basically retained its morphological features, which enabled further ex situ examination by electron microscopy. SEM images of fraction 1, shown in Figure 2a, reveal a smooth, compact, and continuous structure under high magnification. The corresponding AFM topographic image (Figure 2b) establishes the presence of a two-dimensional (2D) structure with a thickness of ca. 80 nm (this value was obtained

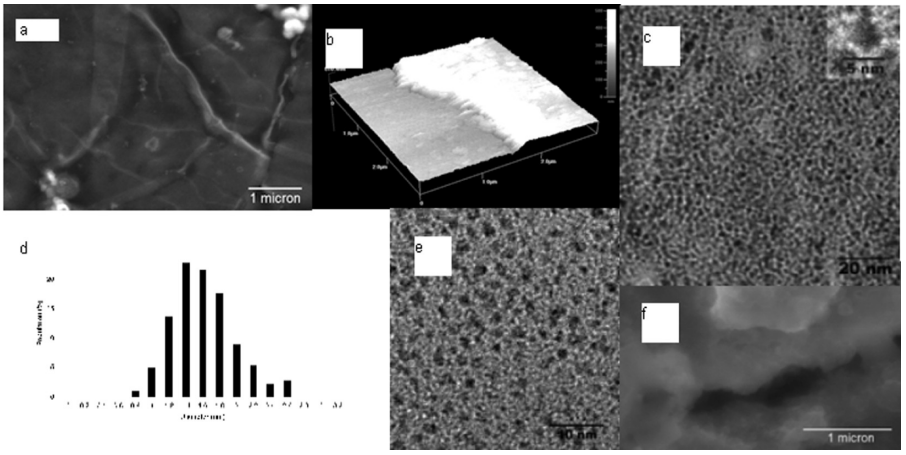

Figure 2. Microstructure of fraction 1 at 24 h of the LLIR operation. (a) SEM image. (b) AFM topographic image. The thickness of the film is measure by peak-to-valley distance as ca. 80 nm. (c) TEM and HRTEM micrographs. The inset indicates that the Au NPs are nanocrystals. (d) Distribution histograph of the particle diameters. (e) Fraction 1 collected at 1.5 h of reaction. (f) SEM micrograph of fraction 3.

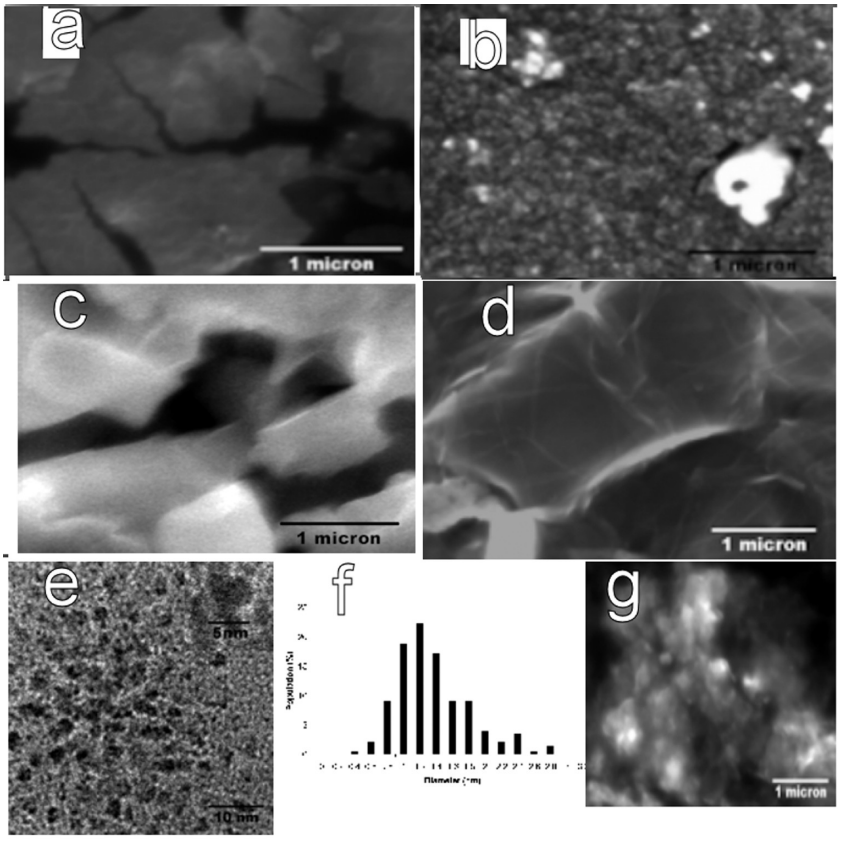

Figure 3. Morphological evolution of deposits. (a) SEM image of the interfacial deposit on reduction of formaldehyde instead of THPC (variation 1a). (b) SEM image of the interfacial deposit on reduction of hydazine instead of THPC (variation 1b). (c) SEM image of interfacial deposit with excess PPh_3 added to the 1.5 mM $Au(PPh_3)Cl$ toluene solution for LLIR (variation 2). (d) SEM image of the interfacial deposit on reduction of hydazine with 1 mM THP, pH = 7.32 (variation 3a). (e) TEM and HRTEM images of the interfacial deposit on reduction of hydazine with 1 mM THP at pH = 7.32. The inset shows that the Au nanoparticles in the film are nanocrystals. (f) Histograph of the particle diameter values from Figure 4e. (g) SEM image of the interfacial deposit on reduction of hydazine with 1 mM THPO, pH = 11.7 (variation 3b).

measuring the maximum peak-to-valley distance). This is in accordance with previously reported results for this system.[19] TEM reveals (Figure 2c) that the film has a compact structure with regular separations (bright network) among Au NPs, with a mean diameter of 1.6 $\pm$ 0.35 nm (N = 228) as illustrated in the histogram plot in Figure 2d. The HRTEM micrograph of fraction 1 (inset of Figure 2c) indicates that the Au NPs inside the network are crystalline. Compared to Figure 2c, which shows a TEM image of the interfacial deposit after a shorter reaction time (1.5 h, Figure 2e), the sample is less dense, suggestive of an increase in Au NP density at the L/L interface with time, in agreement with Rao et al.[19] In contrast, fraction 3 appears to be a three-dimensional solid as illustrated in Figure 2f, suggesting that it differs from fraction 1. Contact angle measurement additionally

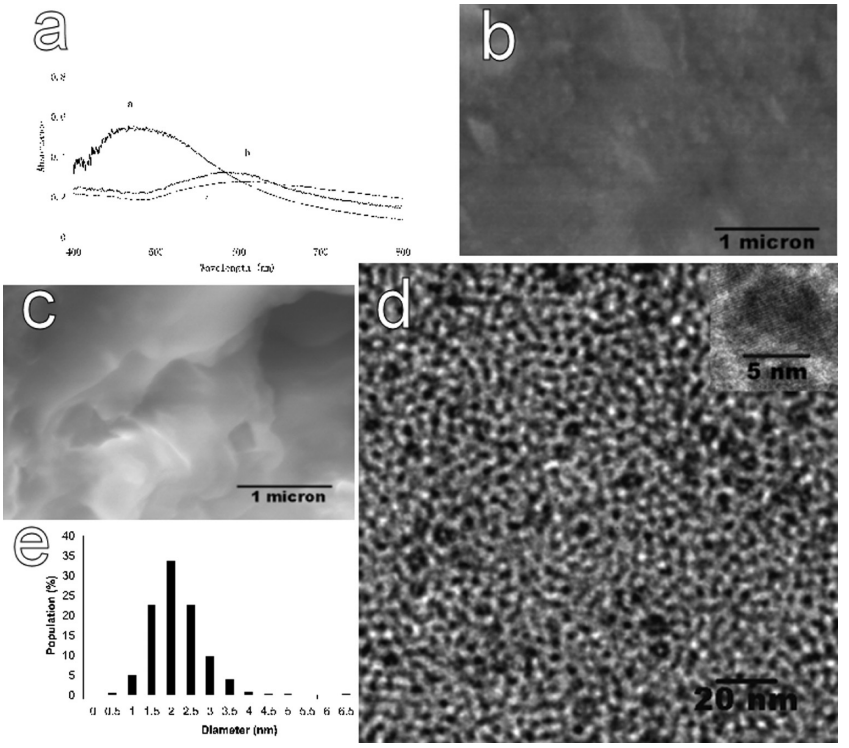

Figure 4. Interfacial products by liquid/liquid interfacial self-assembly (LLSA). (a) UV−vis spectra of the Au aqueous sol (a) and Au films without (b) and with PPh_3 (c) in toluene (variations 1 and 2, respectively). (b) SEM image of the Au film by LLSA variation 1. (c) SEM image of the Au film by LLSA variation 2. (d) TEM image of the Au film by LLSA variation 1. The inset (HRTEM image) indicates that the Au NPs in the film are nanocrystals. (e) Histograph of the particle diameter values from Figure 5d.

indicated there was a difference in surface chemistry between fractions 1 and 3. The average contact angle of water on a clean glass slide, bathed in toluene, was found to be 58.8°, while the values increased to 120.1° and 142.2° when the slides were coated with fractions 1 and 3, respectively (see the Supporting Information). Dynamic measurements of the droplets were also performed to investigate the effect of deposit density on interfacial tension: a distortion of the supported droplets from their initial hemispherical form was seen with time, for both toluene and DCE organic phases (see the Supporting Information).

Variations 1a/1b of the default preparation involved formaldehyde and hydrazine as alternative reducing agents, to perform the LLIR: the deposits were investigated via SEM. A 48 h reduction with formaldehyde produced a thick interfacial layer (Figure 3a); the interfacial deposit from hydrazine reduction is a coarse film (see Figure 3b), highlighting the role of THPC in the formation of 2D films.

Variation 2 of Default LLIR Preparation. When excess PPh_3 (5 mM) was added to the 1.5 mM $Au(PPh_3)Cl$ toluene solution, the SEM micrograph in Figure 3c indicated that the LLIR directly formed a 3D Au solid at the L/L interface instead of a 2D film, reflecting the effect of excess PPh_3 on the morphology.

Variation 3a involved the addition of 1 mM THP to the alkaline hydrazine solution, the resulting interfacial deposit displays a smooth and compact surface again (Figure 3d), and the TEM (Figure 3e) indicates that the interfacial deposit is of analogous structure to fraction 1

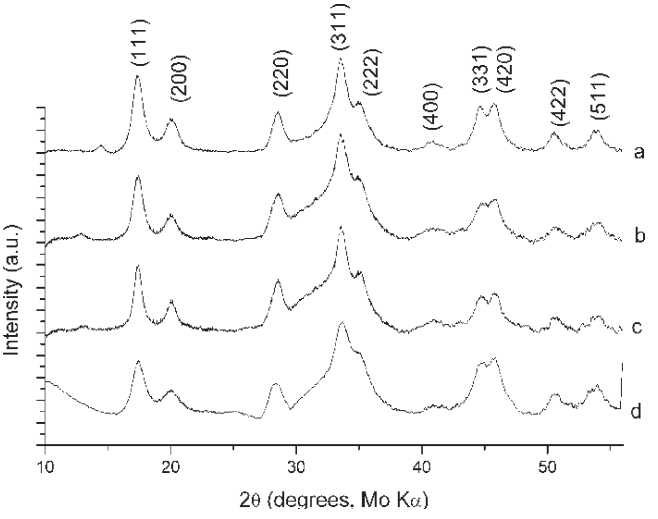

Figure 5. XRD analysis of the interfacial products by different methods. (a) Fraction 1 from LLIR. (b) LLSA variation 1. (c) LLIR variation 3a. (d) LLIR fraction 3.

after 1.5 h of reaction, with a mean diameter of 1.4 ± 0.45 nm ($N = 197$) as illustrated in Figure 3f. The HRTEM micrograph (inset of Figure 3e) also indicates that the interfacial deposit is crystalline. When a THPO solution was used instead of THP (variation 3b), with hydrazine to carry out the LLIR, the SEM observation again shows a bulk aggregate (see Figure 3g).

LLSA Variations 1 and 2. Au NP films can also be prepared by the LLSA method according to methods described previously.[10−12] Here the aqueous Au sol was preformed from the reduction of $NaAuCl_4$ solution with

THPC alkaline solution.[26] The aqueous sol was mixed with the same volume of either toluene (LLSA 1) or 5 mM PPh_3 in toluene solution (LLSA 2), and an interfacial deposit was produced after 1 min of vigorous manual shaking. It was removed to a glass slide for analysis via UV−visible spectroscopy. As shown in Figure 4a, absorption bands centered at wavelengths of ca. 570 nm were obtained for the interfacial deposits produced by both variations of the LLSA procedure, indicative of the formation of Au NP films (c.f. the aqueous Au colloid response in Figure 4a). However, SEM reveals that the two products present different morphologies. LLSA 1 displays a compact and smooth surface (Figure 4b), whereas the addition of PPh_3 in LLSA 2 gave solid aggregates (Figure 4c). The TEM micrograph for the product of LLSA 1 resembles that of LLIR fraction 1 (Figure 4d), with a slightly larger average diameter of 2.13 ± 0.71 nm ($N = 544$), as shown in Figure 4e. HRTEM further indicates that it is a crystalline assembly (see inset of Figure 4d).

Deposit Morphology and Chemical State: XRD and XPS. The broadening of X-ray diffraction peaks provides a rough estimate of crystallite size through analysis with Scherrer's equation:[33]

$$B_{\text{crystallite}} = \frac{k\lambda}{L\cos\theta} \quad (1)$$

where λ is the wavelength of the X-ray, θ is the Bragg angle, L is the average crystallite size measured in a direction perpendicular to the surface of the specimen, and k is a constant and taken as 0.9. The XRD patterns of fractions 1 and 3 from the default procedure, the deposit from variation 3a, and LLSA deposit 1 (toluene only) are presented in Figure 5. Reflections assigned to Au (111), (200), (220), (311), (222), (331), (420), (422), and (511) planes are marked in the plot (*Fm*3*m*, $a = 4.068$ Å, JCPDF no. 02-1095). The crystallite diameters calculated from the (111) reflection are 1.9 nm for fraction 1, 1.6 nm for fraction 3, 2.1 nm for LLIR variation 3a, and 2.0 nm for LLSA variation 1, which indicates that the as-prepared interfacial deposits are nanocrystalline and that fraction 1 can be produced by both approaches, LLSA or LLIR. This highlights the role of capping ligands for the morphological evolution and suggests that the observed LLIR process is actually a combination of interfacial reduction of the Au(I) complex and self-assembly of the resulting Au NPs.

XPS measurements were used to investigate the composition of the capping ligands in the LLIR fractions and the LLSA interfacial deposits. The Au 4f signals of LLIR fractions 1, 2, and 3 and of LLSA interfacial deposits 1 and 2 are plotted in Figure 6a, along with the corresponding curve fits using Gaussian−Lorentzian functions and Shirley backgrounds. In the following, we will only discuss the Au $4f_{7/2}$ spin−orbit component of the spectra, because the Au $4f_{5/2}$ region of the spectra (binding energies > 86 eV) just mirrors the Au$4f_{7/2}$ region with lower emission intensity and does not provide any additional information.

The Au $4f_{7/2}$ emission from fraction 3 is in the binding energy (BE) range of metallic gold (Au^0) at 83.8 eV,[30] but the peak is significantly broadened and asymmetric because of the presence of an additional emission component centered at a BE that is 0.2 eV higher. Similar BE-shifted metallic Au components have been observed previously and are expected for nanoparticulate Au covered by electronegative adsorbates.[30] XRD indicated a mean Au particle size of 1.6 nm for this material (vide supra), and it will be shown below that the P 2p emission from these nanoparticles is likely to stem from electron-withdrawing phosphorus containing capping ligands at their surface. The broadened nature of the Au $4f_{7/2}$ peak likely reflects the presence of a distribution of Au species with varying local coordination, including surface and defect species in the nanoparticulate sample. Moreover, it seems plausible to identify the narrow metallic peak component at 83.8 eV with the fully coordinated bulklike Au sites in the core of the nanoparticles, in line with a very similar interpretation of XPS data for PPh_3-capped Au_{55} clusters[34,35] that are similar in diameter (approximately 2 nm) to the Au nanoparticles examined in this manuscript.

Fraction 1 has two rather broad $4f_{7/2}$ peaks at 84.0 and 85.3 eV, corresponding to the BE ranges of Au^0 and Au^+, respectively.[36,37] This indicates the coexistence of both Au^0 and Au^+. Again, the broadened nature of the peaks suggests the presence of a distribution of species, which is in line with the low mean metal particle size determined by XRD and electron microscopy. It should be noted that some of the Au^0 component in this Au 4f spectrum is due to radiation damage to the sample, because of the observation that prolonged exposure (several hours) of the sample to the X-ray source led to a complete reduction to metallic Au. Exposure of the sample to the laboratory ambient similarly reduced the Au^+ species slowly to Au^0. XPS analysis after storage of fraction 1 for two months indicated that approximately 70% of the Au content in the sample had been reduced to the metallic state.

Fraction 2 presents a strong response of Au^+ at 85.4 eV and a weak feature of Au^0 at 83.8 eV, again suggestive of a mixture of Au^0 and Au^+, which is consistent with the UV−vis analysis. As for fraction 1, radiation damage by the X-rays was observed to cause an increase of the Au^0 peak at the expense of the Au^+ component, but at a significantly lower rate than for fraction 1. XPS analysis after storing fraction 2 for two months in the laboratory ambient also indicated much less conversion of Au^+ to Au^0 than for fraction 1. The cationic species in fraction 2 are much more resistant to reduction, possibly due to protection by the capping ligands.

(33) Suryanarayana, C.; Norton, M. G. *X-ray Diffraction A Practical Approach*; Plenum Press: New York and London, 1998; Vol. *6*, p 213.
(34) Quinten, M.; Sander, I.; Steiner, P.; Kreibig, U.; Fauth, K.; Schmid, G. *Z. Phys. D—Atoms, Mol. Clusters* **1991**, *20*, 377.
(35) Houbertz, R.; Feigenspan, T.; Mielke, F.; Memmert, U.; Harma, U.; Simon, U.; Schön, G.; Schmid, G. *Europhys. Lett.* **1994**, *28*, 641.
(36) Kozlova, A. P.; Kozlov, A. I.; Sugiyama, S.; Matsui, Y.; Asakura, K.; Iwasawa, Y. *J. Catal.* **1999**, *181*, 37.
(37) Knecht, J.; Fischer, R.; Overhof, H.; Hensel, F. *J. Chem. Soc., Chem. Commun.* **1978**, 905.

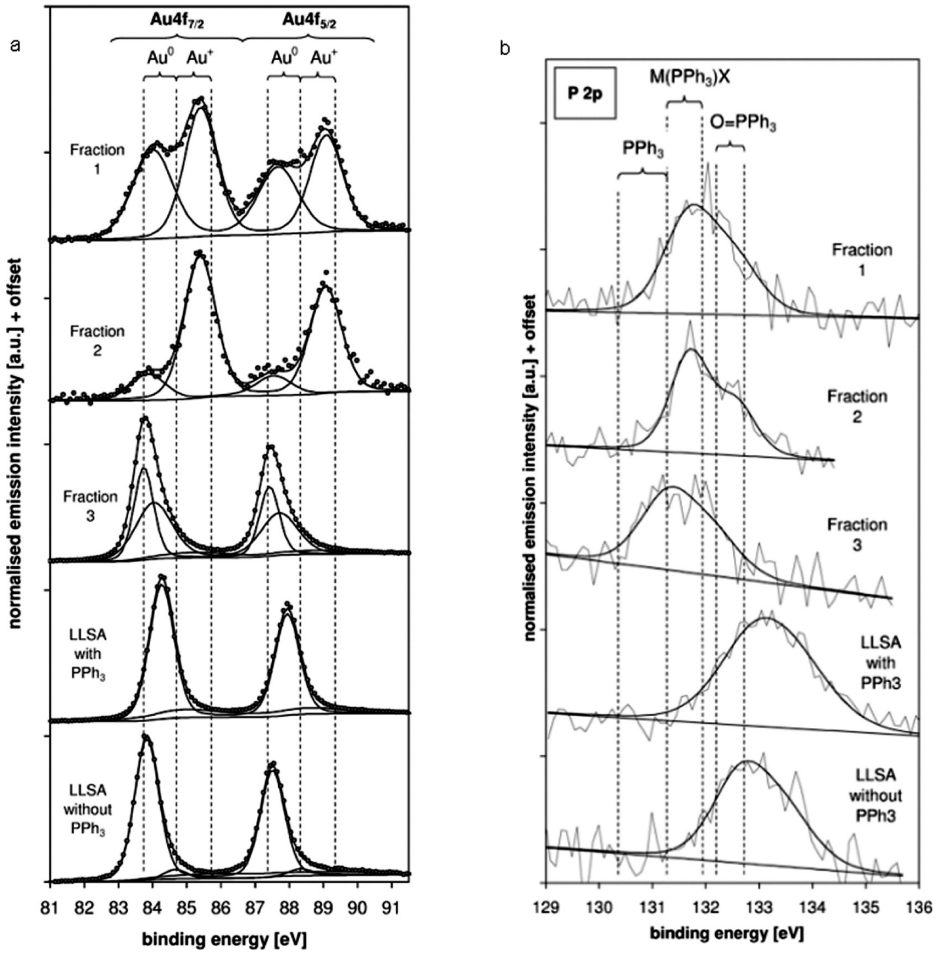

Figure 6. XPS data and results of Gaussian−Lorentzian peak fitting for (from top to bottom): fraction 1, fraction 2 (solid), fraction 3; LLSA variation 2, and LLSA variation 1, where (a) Au 4f emission and (b) P 2p emission. All data are normalized to the height of the strongest peak. Binding energy ranges of reference data are indicated by vertical lines.

The Au signals for LLSA interfacial deposit in toluene (LLSA 1) are characteristic of metallic bulk gold, with a narrow bulklike (fwhm $\sim$ 0.85 eV) Au $4f_{7/2}$ emission at a BE of 83.8 eV (Figure 6a).

An Au 4f emission with similar fwhm but shifted to slightly higher BE (84.2 eV) is displayed when PPh_3 was introduced (LLSA 2). As discussed in the context of the Au 4f results for fraction 3 above, the presence of electron-withdrawing ligands at the surface of Au nanoparticles can have the effect of increasing the Au 4f BE by a few tenths of an electonvolt. Examination of the P 2p emission spectra in the following paragraphs confirms the presence of such an electronegative capping layer, which is attributed to phosphine oxides (specifically THPO).

The P 2p XPS responses are shown in Figure 6b. It is seen that the P 2p emission from fractions 1 (the interfacial deposit) and 2 (the dried solute from the toluene phase) are centered at a BE of approximately 131.7 eV, which is within the BE range previously reported for the P 2p emission from PPh_3 ligands in $Au(PPh_3)Cl$, $Au(PPh_3)_2Cl$, and other organometallic compounds.[36,38−40] Survey XP spectra (not shown) further revealed the presence of almost equal amounts of P and Cl. Together with the presence of Au^+ in the Au 4f data, this indicates that both fractions contain P bound in the form of $Au(PPh_3)Cl$. Some PPh_3 freed by the decomposition of the Au complex to AuCl and PPh_3 might be present as well.

Storing fraction 1 in a laboratory ambient for 2 months led to the appearance of a strong P 2p component at BE values typical for P(V) species, in the BE range above 132.5 eV. This parallels the observation above that any Au^+ present in fraction 1 converted to Au^0 during storage. The appearance of the P(V) component could then be explained by aerial oxidation of PPh_3, freed by the reduction of Au^+, to triphenyl phosphine oxide ($O{=}PPh_3$). This oxidation has been observed in a previous study of $Au(PPh_3)Cl$.[41]

The P 2p emission from fraction 3 is shifted toward a slightly lower BE value of 131.4 eV and approaches the range of previously reported P 2p BEs for free PPh_3,[42] as

(38) Battistoni, C.; Mattogno, G.; Cariati, F.; Naldini, L.; Sgamellotti, A. *Inorg. Chim. Acta* **1977**, *24*, 207.
(39) McNeillie, A.; Brown, D. H.; Smith, W. E.; Gibson, M.; Watson, L. *J. Chem. Soc., Dalton Trans.* **1980**, 767.
(40) Blackburn, J. R.; Nordberg, R.; Stevie, F.; Albridge, R. G.; Jones, M. M. *Inorg. Chem.* **1970**, *9*, 2374.
(41) Uvdal, K.; Persson, I.; Liedberg, B. *Langmuir* **1995**, *11*, 1252.
(42) NIST X-ray Photoelectron Spectroscopy Database, version 3.5 (National Institute of Standards and Technology, Gaithersburg, 2003); http://srdata.nist.gov/xps.

Table 2. Components of the LLIR Product Fractions and LLSA Interfacial Deposits by XPS Analysis

samples	Au $4f_{7/2}$ (eV)	P $2p_{3/2}$ (eV)	solid in the deposits	possible capping ligands
LLIR fraction 1	84.0, 85.3	131.7	Au^0, $Au(PPh_3)Cl$	THP, PPh_3,
LLIR fraction 2	83.8 (weak), 85.4	131.7	Au^0 (weak), $Au(PPh_3)Cl$	PPh_3
LLIR fraction 3	83.8	131.4	Au^0	PPh_3
LLSA variation 1	83.8	133.1	Au^0	THPO
LLSA variation 2	84.2	132.7	Au^0	PPh_3=O, THPO

indicated in Figure 6. Together with the observation of nanoparticulate metallic Au by XRD and Au 4f XPS, this suggests that PPh_3 freed by reduction of Au in the interfacial reaction is associated with a metallic Au deposit at the glass wall of the reaction vessel. Very plausibly, freed PPh_3 acts as a surface capping ligand that facilitates the dissolution in toluene of the Au nanoparticles formed during the interfacial process. These soluble particles then appear to diffuse to the vessel walls, where they seem to aggregate with the PPh_3 capping ligand remaining in the deposit.

The nanoparticulate LLSA product with PPh_3 in toluene (LLSA2) presents a broad P 2p emission line centered around 133.1 eV. This BE is too high for a P(III) species and is higher than the P 2p BEs previously reported for triphenyl phosphine oxides (132.2−132.7 eV {NIST X-ray Photoelectron Spectroscopy Database, version 3.5}) and is therefore very likely to correspond to a P(V) capping species with additional electron withdrawing ligands. The most plausible candidate for this would be $(HOCH_2)_3PO$ [THPO], which is the oxidation product of THPC used in the LLSA process. It has more electronegative ligands than the phenyl groups in the triphenyl phosphine oxide and is thus expected to have a more positive charge on the P center. Interaction with the nanoparticulate Au clusters formed during the interfacial reaction was evident from a shift of the Au 4f emission (see above) and is likely to cause an additional shift of the P 2p BE to higher values. Such a shift would also be likely for $O{=}PPh_3$ adsorbed on the Au nanoparticles, so it is possible that adsorbed THPO and $O{=}PPh_3$ might coexist in this sample.

By contrast, the P 2p signal for the LLSA product 1 appears at a slightly lower BE of 132.7 eV, at the upper end of the range of previously reported values for triphenyl phosphine oxide. This suggests that the P signal also stems from THPO, interacting with the surface of the bulklike Au deposits formed in the LLSA process in the absence of PPh_3.

To summarize the XPS analysis, all results for the Au 4f and P 2p emission analysis are brought together in Table 2. The Au^+ in the deposits should be in form of $Au(PPh_3)Cl$, according to Woehrle et al.,[42] who found in similar experiments that as-reduced Au NPs were covered by a "shell" of $Au(PPh_3)Cl$. Fraction 1 of the LLIR product is probably a mixture of metal Au and $Au(PPh_3)Cl$, together with capping ligands of PPh_3 and THP derived from the reducing agent. The metallic Au content in fraction 2 is very low relative to $Au(PPh_3)Cl$, and PPh_3 is suggested to be a capping ligand that provides a hydrophobic "shell" outside the solid Au and $Au(PPh_3)Cl$. Fraction 3 is simply metallic Au nanoparticles capped with PPh_3. The product from LLSA variation 1 (pure toluene) exhibits the combined presence of bulklike metallic Au and the THPO species, while the LLSA product from variation 2 (with PPh_3) in toluene is identified as metallic Au, with THPO (possibly coexisting with PPh_3=O) present as a capping ligand that causes a shift of the Au $4f_{7/2}$ binding energy. Compared to the LLSA (interfacial nanoparticle assembly) with pure toluene, the reduction of the Au(I) complex for the LLIR fraction 1 is apparently incomplete, which leads to the smaller crystallite size of Au^0 covered by a shell of $Au(PPh_3)_xCl$.

Regarding the source of the capping ligands, $Au(PPh_3)Cl$ in toluene is able to release PPh_3 when it is reduced to Au^0 at the L/L interface, but the ligand can be trapped by $Au(PPh_3)Cl$ from the organic solution, to generate $[Au(PPh_3)_2]^+Cl^-$ in a side reaction or it can attach to the formed Au NPs to give the "shell" of $Au(PPh_3)Cl$.[43] Hence, no free PPh_3 would remain in the toluene phase in the initial stage of LLIR. However, free PPh_3 can become available when the $Au(PPh_3)Cl$ is depleted over time by its reduction. The experiments with excess PPh_3 in toluene (variation 2 and LLSA variation 2) therefore probably simulate the latter stages of the LLIR, which is also indicated by the fact that the interfacial deposits possess similar morphology to fraction 3.

Deposit Characterization: Breakdown Products of Reducing Agents. The cleavage of THPC is another source of phosphorus-based capping ligands. When the pH value is sufficiently high, the following decomposition of THPC was proposed by Grayson:[44]

$$(HOCH_2)_4PCl + NaOH \rightarrow (HOCH_2)_3PO + CH_2O + NaCl + H_{2(g)} \quad (2)$$

However, when the THPC is neutralized stoichiometrically by OH^-, $(HOCH_2)_3P$ (THP) and formaldehyde are produced without releasing hydrogen gas:[44]

$$(HOCH_2)_4PCl + NaOH \rightarrow (HOCH_2)_3P + CH_2O + NaCl + H_2O \quad (3)$$

THP can be oxidized to THPO with a half reaction time of 30 min at pH 10, but it is stable at pH 7 over 24 h.[23] It is also possible to form more complex compounds, such as the mono- and dihemiformals of THP and THPO[45]

(43) Woehrle, G. H.; Brown, L. O.; Hutchison, J. E. *J. Am. Chem. Soc.* **2005**, *127*, 2172.
(44) Grayson, M. *J. Am. Chem. Soc.* **1963**, *85*, 79.
(45) Ellzey, S. E.; Connick, W. J. *Am. Dyestuff Rep.* **1973**, *62*, 47.

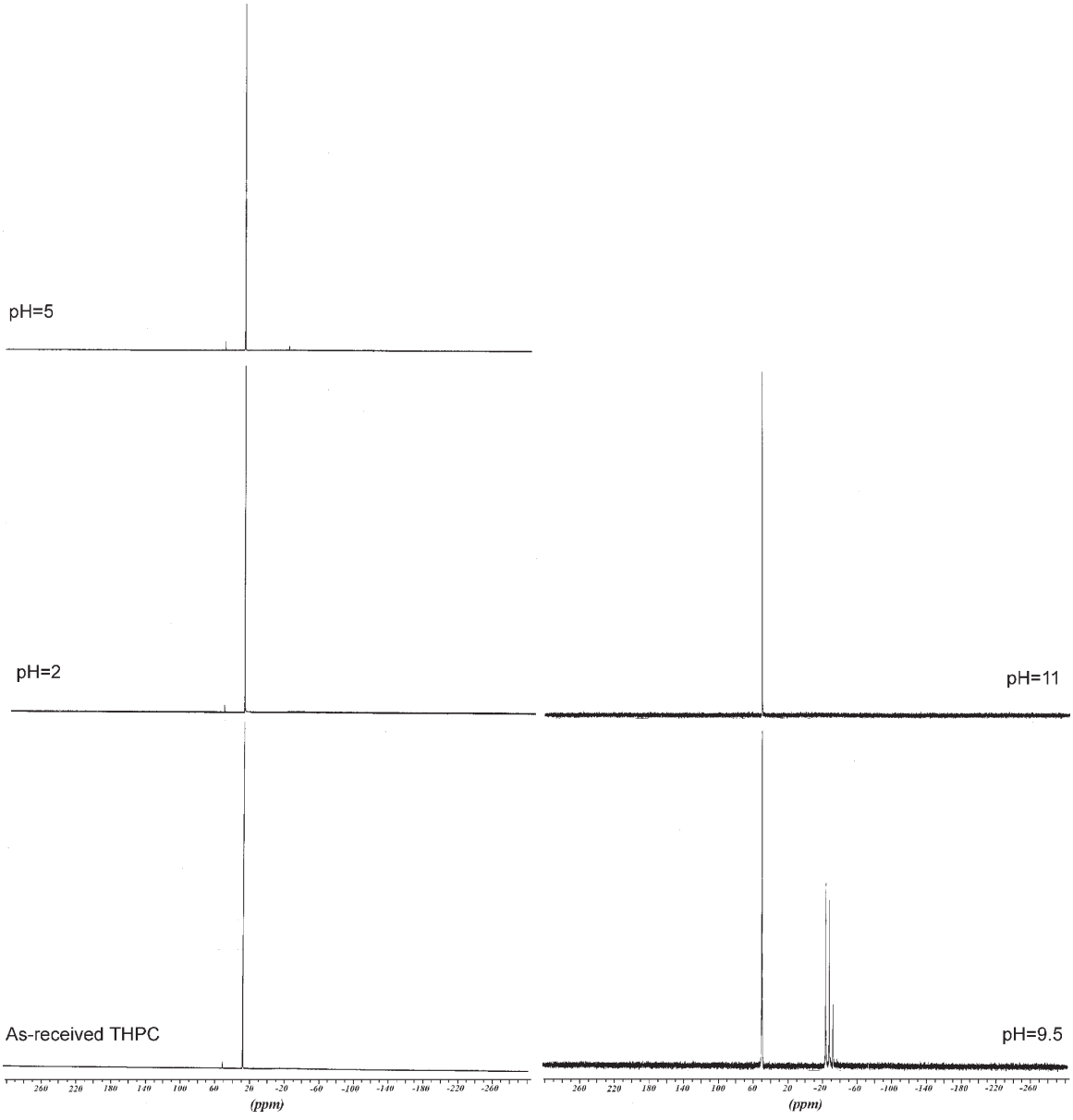

Figure 7. ^{31}P NMR spectra obtained for aqueous solutions of THPC as a function of pH.

postulated by Vullo:[46]

$$(HOCH_2)_3P+$$
$$(HOCH_2)_3PO \overset{CH_2O}{\leftrightarrow} (HOCH_2)_{3-n}P(CH_2OCH_2OH)_n+$$
$$(HOCH_2)_{3-n}PO(CH_2OCH_2OH)_n \qquad (4)$$

The cleavage of THPC as a function of pH was investigated via ^{31}P NMR spectroscopy. As shown in Figure 7, the as-received THPC solution (80% water solution) exhibits a strong resonance at 26.9 ppm and a weak one at 50.2 ppm, which are indicative of the major component (THPC) and trace THPO, according to previous reports.[45,47] At pH 2, there is no change in the ^{31}P NMR response. An additional very weak signal appears at −23.4 ppm when the pH value reaches 5, which is attributed to the existence of THP.[45] The peak shifts of THPC solutions may be due to the use of lithium hydroxide instead of sodium hydroxide as the base.[45,47] The THPC solution at pH 9.5 displays complicated responses where the THPC resonance has disappeared. Instead, two large signals are seen at 50.2 ppm and −23.3 ppm, attributed to THPO and THP, respectively, together with two additional peaks at −27.5 ppm and a smaller resonance at −31.7 ppm, which are possibly due to the complex mono- or dihemiformals of THP and THPO. When the pH was increased to 11, only the resonance at 52.4 ppm was seen, which is assigned to THPO: hence, THPC is stable at lower pH (≤2). When the pH value is increased, the first cleavage product is THP, and all the cleavage products are ultimately oxidized to THPO in alkaline solution, which is in accordance with the previous literature.[24]

Information on the time-scale of the cleavage is obtained through a cyclic voltammetric (CV) investigation,

(46) Vullo, W. J. *J. Org. Chem.* **1968**, *33*, 3665.
(47) Frank, A. W.; Daigle, D. J.; Vail, S. L. *Textile Res. J.* **1982**, *52*, 738.

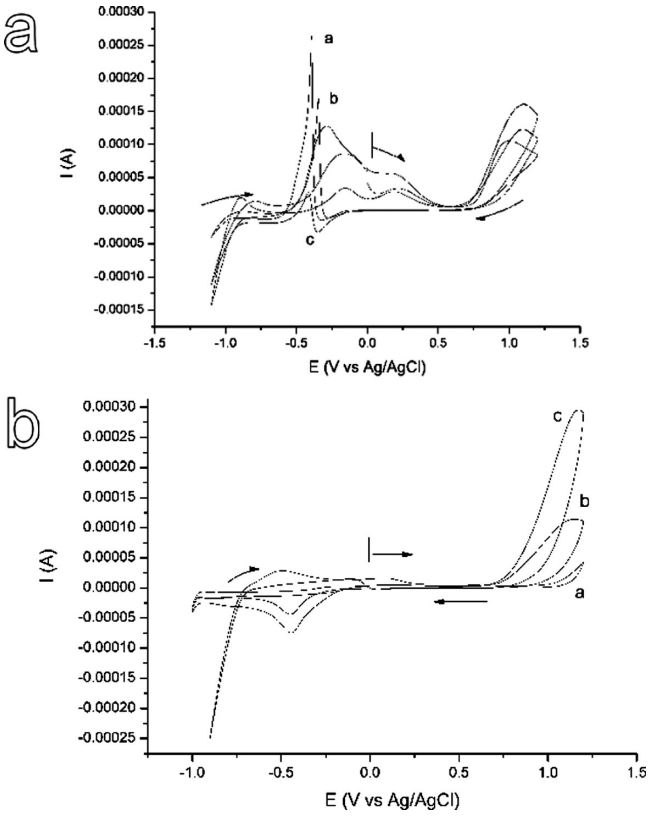

Figure 8. Time-dependence of cyclic voltammetric scans. (a) 10 mM formaldehyde in 100 mM LiCl and 31.25 mM NaOH solutions: (a) fresh solution, (b) after 40 min, and (c) after 17 h. (b) 10 mM THPC in 100 mM LiCl and 31.25 mM NaOH solutions: (a) fresh solution, (b) after 25 h, and (c) CVs without THPC in the solution.

carried out on 10 mM formaldehyde and THPC in 31.25 mM NaOH and 100 mM LiCl solution, because formaldehyde is accepted as one of the products of cleavage and it functions as a reducing agent for Au^{+} or Au^{3+} species. The time-dependence is shown in Figure 8, where the CV responses of formaldehyde become weaker with time due to its decomposition, in accordance with previous reports.[48] For the THPC alkaline solution, no strong features are seen in the CV scans for both the freshly prepared THPC alkaline solution and the one after 3 h, and also no peaks corresponding to free formaldehyde appear, indicating that THPC in the alkaline solution is not electroactive due to rapid oxidation and the cleavage products are possibly mono-, di-, or trihemiformals.

Conclusions

The identity of the LLIR product was found to vary with reaction time and the location in the reactor, where three distinguishable fractions are obtained. Fraction 1 is composed of Au NPs with regular separation from each other because of the presence of the organic ligands, fraction 2 is basically a mixture of Au(I) complex and small amount of Au NP suspension, and fraction 3 is particulate Au capped with PPh_3 ligands. Particles with similar morphology to fractions 1 and 3 can be formed by self-assembly, where an Au hydrosol is adsorbed to the liquid/liquid interface although the surface ligands are present in a more oxidized state.

It is clear that the LLIR is a complex process, which combines the reduction of $Au(PPh_3)Cl$ at the L/L interface with the self-assembly of the as-prepared Au NPs into ultrathin films. In the beginning, the $Au(PPh_3)Cl$ is most likely to encounter the hemiformals of THP and formaldehyde at the L/L interface, and the Au^{+} is reduced by THP or formaldehyde. The P^{3+} species can either be derived from the $Au(PPh_3)Cl$ shell[43] of the as-formed Au NPs, or from the rest of the THP adsorbed on the surface, since the formaldehyde released from the hemiformals (eq 4) can also reduce Au^{+}. The reduction of $Au(PPh_3)Cl$ liberates PPh_3 molecules, where only a fraction can attach on the Au NPs as a shell. The rest combine with $Au(PPh_3)Cl$ molecules in the toluene solution to form $[Au(PPh_3)_2]^{+}Cl^{-}$ as suggested.[43] Formaldehyde can serve as the main reducing agent, on the depletion of THPC, and it can sustain an adequate reaction rate because the existence of as-formed Au NPs at the L/L interface catalyze the decomposition of formaldehyde.[49] Therefore the site of the reduction will remain at the surface of as-formed Au NPs, which leads to the growth of the NPs. The THPO, like the analogous capping agent tri-*n*-octylphosphine oxide (TOPO),[50,51] has a weaker interaction than PPh_3 with Au NPs, so the as-formed Au deposit is mainly capped by PPh_3 (the P^{3+} species indicated by XPS results), which is more hydrophobic than fraction 1, as indicated by the contact angle measurements. The surface of some Au NPs may even be entirely capped by PPh_3 and $AuPPh_3$ to form Au suspensions in the toluene phase, which constitute fraction 2. Excess PPh_3 causes aggregation of this product, the fraction is then able to adsorb on the glass tube, leading to deposition as fraction 3.

Particle size and adsorption behavior are thus intimately linked to surface chemistry and, in the specific system investigated here, to the presence and nature of P-containing species. The presence of polar P ligands (THP and/or THPO) correlates with the formation of regular, two-dimensional NPs in the LLIR and LLSA preparations, indicating that the polar character of the ligands renders the NPs surface active (see contact angle measurement). By contrast, the presence of less polar PPh_3 ligands (either added deliberately or built up in the latter stages of reaction) leads to a more hydrophobic particle surface. This in turn leads to the detachment of the particles to the organic phase, or to their adsorption on the vessel walls, and hence the resultant three-dimensional structures observed on extracting these fractions from solution.

The LLIR has been presented as a general method for preparing ultrathin films of metals, alloys, metal chalcogenides, and oxides.[19,23,52] The mechanistic details

(48) ten Kortenaar, M. V.; Kolar, Z. I.; de Gopeij, J. J. M.; Frens, G. *J. Electrochem. Soc.* **2001**, *148*, E327.
(49) Jia, M. L.; Shen, Y. N.; Li, C. Y.; Bao, Z.; Sheng, S. S. *Catal. Lett.* **2005**, *99*, 235.
(50) Green, M.; O'Brien, P. *Chem. Commun.* **2000**, 183.
(51) Harnack, O.; Ford, W. E.; Yasuda, A.; Wessels, J. M. *Nano Lett.* **2002**, *2*, 919.
(52) Rao, C. N. R.; Kulkarni, G. U.; Thomas, P. J.; Agrawal, V. V.; Gautam, U. K.; Ghosh, M. *Curr. Sci.* **2003**, *85*, 1041.

obtained for the LLIR of Au film formation should also provide insight into the formation of other materials by L/L interfacial reactions.

Acknowledgment. The authors are thankful for financial support from the U.K. Engineering & Physical Science Research Council (EPSRC, grant reference EP/C509773/1 and EP/E000665/1), ESF COST workgroup D36/005/06, and for analytical assistance from Dr. Patrick Hill, Mr. Andrew Ballantyne, and Mr. Dan Bradley on TEM, ^{31}P NMR, and AFM, respectively. We are grateful to Dr. John Walton for his continuing technical support and maintenance of the XPS instrument.

Supporting Information Available: Images of an aqueous drop on a clean glass slide and slides coated fractions 1 and 3. Also shown are the evolution of four drops recorded with the LLIR in toluene, and one DCE drop in aqueous solution, as a function of time. This material is available free of charge via the Internet at http://pubs.acs.org.